Front. Optoelectron. 2015, 8(4): 402–412
DOI 10.1007/s12200-015-0497-8

RESEARCH ARTICLE

Error compensation for three-dimensional profile measurement system

Xu YE[1], Haobo CHENG (✉)[1], Zhichao DONG[1], Hon-Yuen TAM[2]

1 School of Optoelectronics, Beijing Institute of Technology, Beijing 100081, China
2 Department of Mechanical and Biomedical Engineering, City University of Hong Kong, Hong Kong, China

Abstract Three-dimensional (3D) profile measurement is an indispensable process for assisting the manufacture of various optic, especially aspheric surfaces. This work presents the measurement error calibration of a 3D profile measurement system, namely PMI700. Measurement errors induced by measuring tool radius, alignment error and the temperature variation were analyzed through geometry analysis and simulation. A quantitative method for the compensation of tool radius and an alignment error compensation model based on the least square method were proposed to reduce the measurement error. To verify the feasibility of PMI700, a plane and a non-uniform hyperboloidal mirror were measured by PMI700 and interferometer, respectively. The data provided by two systems were high coincident. The direct subtractions of results from two systems indicate RMS deviations for both segments were less than 0.2λ.

Keywords aspheric surface, three-dimensional (3D) profile measurement, alignment error, error compensation

1 Introduction

Aspheric elements are widely used in modern optical systems, such as high power laser weapon, space telescope, infrared camera etc, due to its advantages in correcting aberration, expending the field of view and simplifying the structure of optical system in contrast to traditional optical elements. However, the difficulty of aspheric surface measurement has limited its application.

The measurement methods of aspheric surface have been developed maturely in the basis of different principles, e.g., geometrical optics, interferometry and profile measurement, which are listed in Table 1. For specular aspheric surface, these methods are quite suitable. Nevertheless, for a rough (i.e., non-specular) surface, the methods of using laser interferometry cannot make function well. One candidate is infrared interferometer [9]. However, it is 1) expensive due to its precious infrared devices; 2) low sensitivity because of the longer laser wavelength (e.g., 10.6 μm for CO_2 laser); 3) still dependent on null compensators for measuring aspherics. Commercialized coordinate measurement machine (CMM) is also an alternative. Form Talysurf PGI 1240 (Taylor Hobson) is commonly used for measuring surface profile, but its gauge range (~12.5 mm) and traverse range (~200 mm) are not enough for large aspherics (e.g., meter-scale). The multi-probe bar profilometer developed by Itek [10] utilizes a high precision sphere and multi-linear variable differential transformer (multi-LVDT) sensors for comparison measurement, which has accuracy of 0.15 μm RMS (root mean square). However, it needs a high precision reference sphere, which is costly and complex. Comley et al. [11] and Gray et al. [12] reported the profile data of European Extremely Large Telescope (E-ELT) segments (1.4 m size) measured by an off-machine Leitz CMM. Su et al. [13,14] investigated a swing arm profilometer for *in situ* measurement of aspherics. The machine adopts sphere coordinate and can be calibrated by dual probe, which achieves the sub-micron accuracy. Jing et al. [15,16] also reported a swing arm profilometer. They employed a model to raise accuracy to 0.2 μm. Researchers also have developed on-machine measurements for increasing fabrication efficiency [17].

This paper presents a three-dimensional (3D) profile measurement system (PMI700) which can be used for aspheric surface measurement. The measurement errors induced by tool radius, alignment error and temperature variation are analyzed through geometry analysis and simulation. In Section 3, a quantitative method for the compensation of tool radius and an alignment error compensation model based on the least square method have been presented. Plane mirror and non-uniform

Received December 5, 2014; accepted April 9, 2015

E-mail: chenghaobo@tsinghua.org.cn

Table 1 Common measurement methods of aspherics

Principle		method
geometrical optics		knife-edge test [1], Hartmann method [2], Ronchi method [3], etc
interferometry	null testing	aberration-free point, optical holography, computer generated hologram (CGH) [4], Moiré fringe [5], etc
	non null testing	sub-aperture stitching [6], dual-wavelength holography [7], shearing interferometry [8], etc
profile measurement		coordinate measurement machine (CMM), etc

hyperboloidal mirror were measured by PMI700 in Section 4, to verify the practicability of PMI700.

2 Background of profile measurement

2.1 Aspheric surfaces

Aspheric surfaces frequently-used in optical systems can be expressed as Eq. (1), where C denotes the curvature of aspherics ($C = 1/R$, R is vertex radius of curvature), K is conic constant, n refers to the aspheric order, A_{2i} indicates the high order aspheric coefficient.

$$Z(X,Y) = \frac{C(X^2+Y^2)}{1+\sqrt{1-(K+1)C^2(X^2+Y^2)}} + \sum_{i=1}^{n} A_{2i}(X^2+Y^2)^i. \tag{1}$$

As off-axis aspherics are now popular in spaced three reflective cameras, collimating devices, etc, increasing attention has been paid to it. Generally speaking, there are two types of off-axis aspherics as shown in Fig. 1. One is an off-center portion of a symmetric parent mirror (OA-I), and the other is cut from OA-I which seems symmetric (OA-II). The surface equation of OA-I in $O_1-X_1Y_1Z_1$ is defined as Eq. (2), where (y_0,z_0) refers to the coordinate of O_1 in the parent mirror. The surface definition of OA-II can be obtained by rotating Eq. (2) along X_1-axis with a rotating angle θ. According to the coordinate transform theory, point (X',Y',Z') should satisfy Eq. (3). Combining Eqs. (2) and (3) yields Eq. (4) , and it can be simplified as Eq. (5), which is the theoretical surface equation of OA-II.

$$Z_1(X,Y) = \frac{C\left(X_1^2+(Y_1-y_0)^2\right)}{1+\sqrt{1-(K+1)C^2\left(X_1^2+(Y_1-y_0)^2\right)}} - z_0, \tag{2}$$

$$\begin{vmatrix} X' \\ Y' \\ Z' \\ 1 \end{vmatrix} = \begin{vmatrix} 1 & 0 & 0 & 0 \\ 0 & \cos\theta & -\sin\theta & 0 \\ 0 & \sin\theta & \cos\theta & 0 \\ 0 & 0 & 0 & 1 \end{vmatrix} \begin{vmatrix} X_1 \\ Y_1 \\ Z_1 \\ 1 \end{vmatrix}, \tag{3}$$

$$AZ'^2 + BZ' + Q = 0, \tag{4}$$

$$Z' = \frac{-B+\sqrt{B^2-4AQ}}{2A}, \tag{5}$$

where,

$$\begin{cases} A = C + KC\cos^2\theta, \\ B = (-2CY'\sin\theta\cos\theta - 2Cy_0\sin\theta - 2\cos\theta \\ \quad +(K+1)C(2z_0\cos\theta + 2Y'\sin\theta\cos\theta)), \\ Q = 2z_0 + 2Y'\sin\theta - (K+1)C\left(z_0^2 + 2Y'z_0\sin\theta\right) \\ \quad +Y'^2\sin^2\theta) - C(X'^2 + Y'^2\cos^2\theta \\ \quad +2Y'y_0\cos\theta + y_0^2). \end{cases} \tag{6}$$

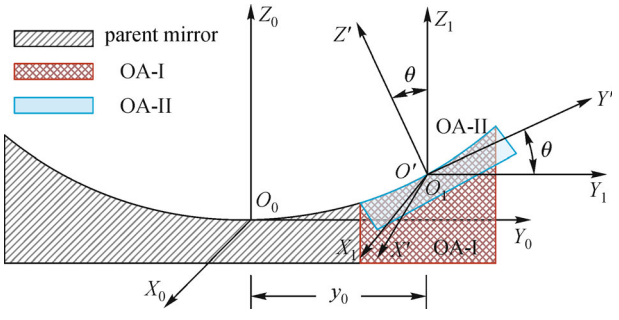

Fig. 1 Sketch map of aspheric surfaces

2.2 Three-dimensional profile measurement system PMI700

PMI700 (Fig. 2) is a precision measurement system for optical elements, especially for aspherics. Its main function includes 1) on line measurement, 2) data analysis and processing. It adopts gantry structure on a base marble of 1780 mm × 1160 mm × 860 mm, and comprises three main parts: XZ axis (stroke: 700 mm × 200 mm), a 600 mm rotating turntable (C-axis) supporting workpieces, and a changeable metrology unit with a length gauge attached at the end of Z-axis.

A commercially available digital length gauge MT60 (HEIDENHAIN) with a touch-trigger probe is mounted as a contact sensor. MT60 employs an optical linear encoder to measure the extended length of its plunger with maximal

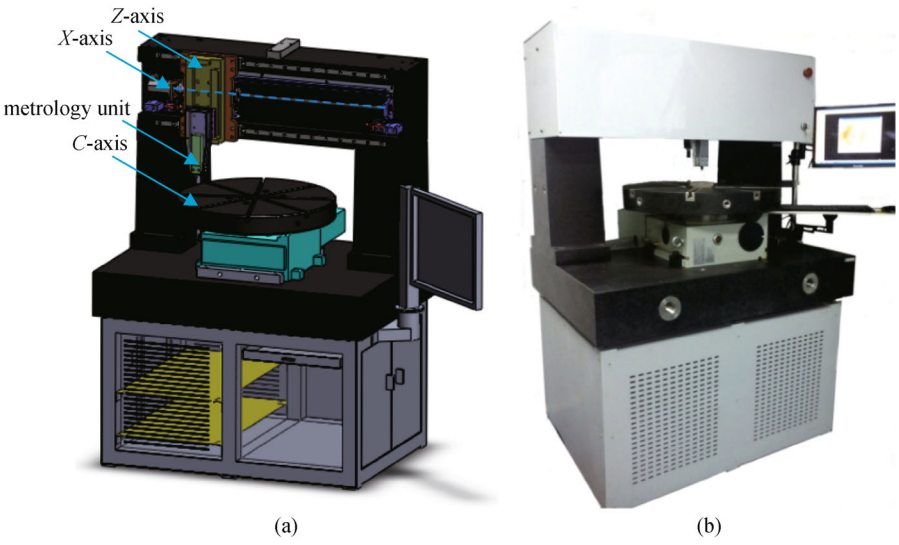

Fig. 2 Schematic of PMI700. (a) CAD model of PMI700; (b) entity of PMI700

stroke of 60.8 mm, which is larger than the maximal sagittal height of most meter-scale spheres and aspherics. Therefore, the *Z*-axis can keep dormant during measurement, which eliminates errors induced by the positioning error of *Z*-axis.

2.3 Path planning of aspherics measurement

Based on the mechanical structure of PMI700, this measurement system can realize three types of path planning, i.e., meridian line (Fig. 3(a)), concentric circles (Fig. 3(b)) and helical line path (Fig. 3(c)). The meridian line path can recover the aspheric surface with few measuring points, estimate the vertex radius of curvature and conic constant of aspherics conveniently, and improve the fitting precision of the processing program. However, this path type should be equipped with high precision turntable to realize the measurement in different direction. In addition, the retrace error of the turntable would be introduced easily during the reciprocating motion of *X*-axis. Concentric circles path can avoid the retrace error, but it would produce deviation during the estimation of vertex curvature radius and conic constant. Helical line path is inefficiently due to a great deal of measuring points, while its measuring accuracy improves obviously compared with the other two path types.

On the basis of the described above, meridian line and concentric circles path have high efficiency and low precision, while helical line path is just the opposite. Thus, the first two types can be used for the measurement during the manufacture of the aspherics, while helical line path apply to the estimation of the profile quality.

3 Calibrations and alignments of PMI-700

Through improving the mechanical precision of the system usually has little effect on the improvement of the measurement accuracy. In order to obtain an excellent measurement result inexpensively and effectively, error

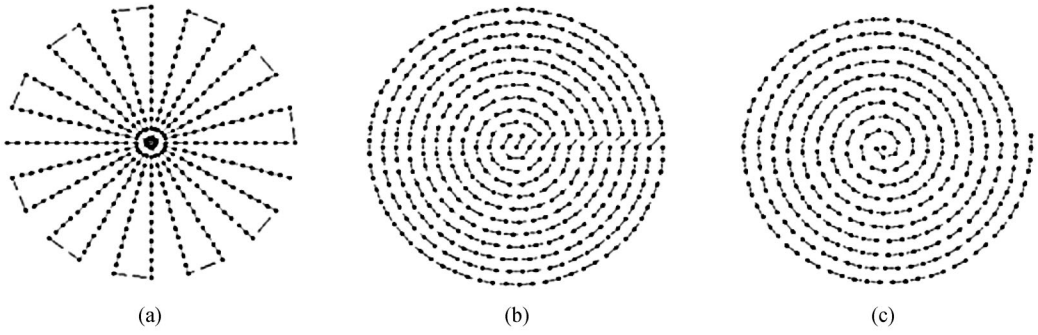

Fig. 3 Path of profile measurement. (a) Meridian line path; (b) concentric circles path; (c) helical line path

compensation technique has been widely used in the three-dimensional profile measurement system. Applying the theoretical error compensation model to the data processor of PMI700, the measurement error would be corrected basically. This paper would analyze error compensation models under different conditions as follows.

3.1 Compensation of tool radius

As the model illustrated in Fig. 4, due to the tool tip has a sphere with radius R_t = 1.6 mm, the factual contact point Q on the curved surface is not the point to be measured (point P), and the length gauge gives the sagittal height of point U (the lowest point of the sphere), which consequently induces nonlinear error in measurement results. That is, there exists an inconformity between theoretical and actual measuring point, which would generate great impact on the fitting result of vertex curvature radius and the second-order coefficient. Hence, it is necessary to compensate the error of tool radius.

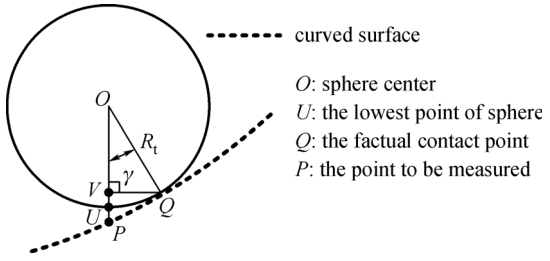

Fig. 4 Compensation of tool radius

A common method to eliminate this error is adding or subtracting the theoretical sagittal deviation of point U and P as shown in Eq. (7), where, X_P, Y_P are given by the measurement path, Z_Q, Z_P can be given by Eq. (1), and γ is the included angle of the normal vector of Q and Z-axis. Moreover, the tip sphere is made of special hard-wearing steel and can be replaced by a new one. Thus, tool wear is not considered.

$$\begin{aligned} Z_{UP} &= Z_{VP} - Z_{VU} = Z_Q - Z_P - Z_{VU} \\ &= Z\left(\sqrt{(X_P^2 + Y_P^2)} + R_t \sin\gamma, 0\right) \\ &\quad - Z\left(\sqrt{(X_P^2 + Y_P^2)}, 0\right) - R_t(1 - \cos\gamma). \end{aligned} \tag{7}$$

3.2 Model of alignment error

The traditional method to calibrate the positioning error is, adjusting the center of the workpiece in accordance with the origin of the measuring tool and eliminating the tilt error of the result. As the center of the workpiece and the measuring tool cannot be in alignment absolutely, and the adjustment of the workpiece would expend a lot of time, this method can be only used in the condition of low precision. Alignment error, i.e., translation error, includes the error between measuring tool and workpiece, measuring tool and turntable, and workpiece and turntable. Here, the models of these three situations would be studied in the following.

3.2.1 Model of alignment error between measuring tool and workpiece

Assuming the alignment error of the workpiece relative to the measuring tool is $(\mathrm{d}x,\mathrm{d}y)$ as shown in Fig. 5(a), and there is no alignment error between measuring tool and turntable. With the translation of the workpiece along X-axis, the aspheric surface can be denoted as

$$z' = \frac{c\left((x-\mathrm{d}x)^2 + (y-\mathrm{d}y)^2\right)}{1 + \sqrt{1-(1+k)c^2\left((x-\mathrm{d}x)^2 + (y-\mathrm{d}y)^2\right)}}. \tag{8}$$

Thus, the measurement error $\mathrm{d}z_{(\mathrm{d}x,\mathrm{d}y)}$ induced by the alignment error $(\mathrm{d}x,\mathrm{d}y)$ can be written as

$$\begin{aligned} \mathrm{d}z_{(\mathrm{d}x,\mathrm{d}y)} &= z' - z \\ &= \frac{c\left((x-\mathrm{d}x)^2 + (y-\mathrm{d}y)^2\right)}{1 + \sqrt{1-(1+k)\left)c^2\left((x-\mathrm{d}x)^2 + (y-\mathrm{d}y)^2\right)}} \\ &\quad - \frac{c(x^2+y^2)}{1 + \sqrt{1-(1+k)c^2(x^2+y^2)}}. \end{aligned} \tag{9}$$

It can be simplified as

$$\begin{aligned} \mathrm{d}z_{(\mathrm{d}x,\mathrm{d}y)} &= -\frac{cx}{\sqrt{1-(1+k)c^2(x^2+y^2)}}\mathrm{d}x \\ &\quad - \frac{cy}{\sqrt{1-(1+k)c^2(x^2+y^2)}}\mathrm{d}y. \end{aligned} \tag{10}$$

Supposing the measuring path is grating, $\mathrm{d}x = \mathrm{d}y = -0.2$ mm, the 3D alignment error distribution of a round workpiece with radius $r = 20$ mm can be seen in Fig. 5(b).

3.2.2 Model of alignment error between measuring tool and turntable

The alignment error between measuring tool and turntable generally exists in the polar coordinate measuring path, which means the measuring tool moving along X-axis and rotating with the turntable at the same time. The measuring model can be seen in Fig. 6(a).

For the theoretical measuring point $A(r,\theta)$, the practical

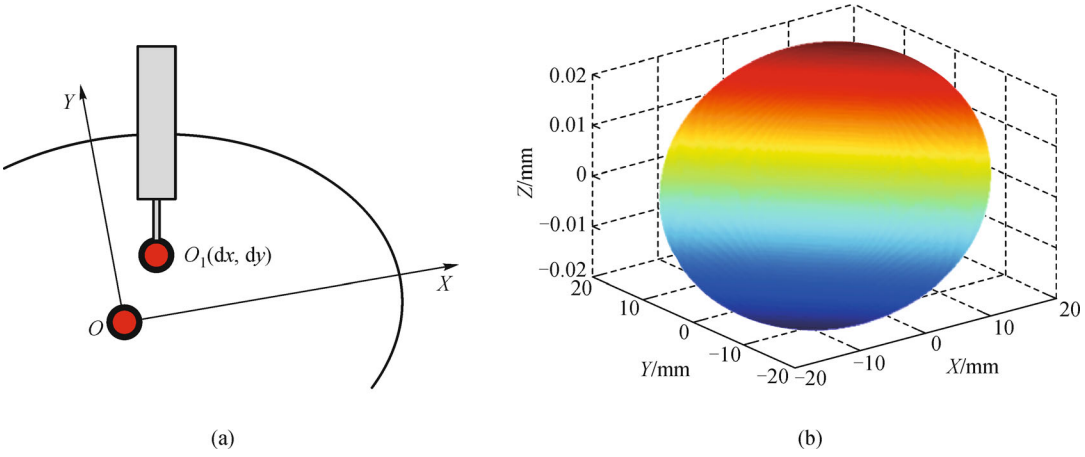

Fig. 5 Model of alignment error between measuring tool and workpiece. (a) Geometrical relationship of alignment errors; (b) 3D distribution of alignment error

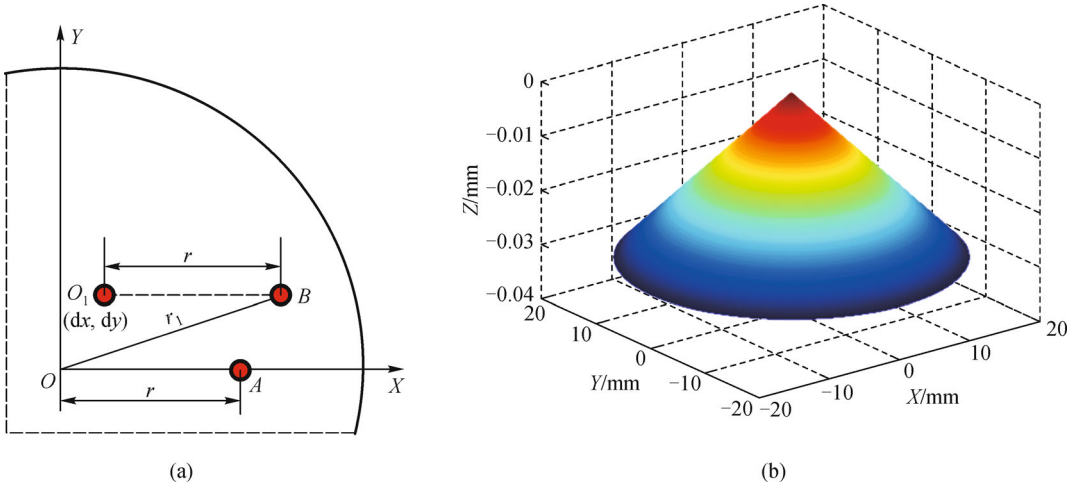

Fig. 6 Model of alignment error between measuring tool and turntable. (a) Geometrical relationship of alignment errors; (b) 3D distribution of alignment error

measured position is located in point $B(r+\mathrm{d}x,\mathrm{d}y)$ if the aligned position of measuring tool and turntable is $O_1(\mathrm{d}x,\mathrm{d}y)$. Based on the geometrical relationship, the measurement error can be obtained as follows

$$\mathrm{d}z_{(x,y)} = \frac{c\left((r+\mathrm{d}x)^2+\mathrm{d}y^2\right)}{1+\sqrt{1-(1+k)c^2\left((r+\mathrm{d}x)^2+\mathrm{d}y^2\right)}} - \frac{cr^2}{1+\sqrt{1-(1+k)c^2r^2}}, \tag{11}$$

and simplified into

$$\mathrm{d}z_{(x,y)} = \frac{cr}{\sqrt{1-(1+k)c^2r^2}}\mathrm{d}x. \tag{12}$$

From Eq. (12), it can be seen the measurement error induced by alignment error is proportional to polar radius r, and only influenced by error $\mathrm{d}x$ along X-axis. If the measuring path in polar coordinate is moving along Y-axis, $\mathrm{d}x$ should be replaced by $\mathrm{d}y$ in Eq. (12). Simulating the measurement error induced by alignment error with parameters $\mathrm{d}x = -0.5$ mm, $r = 20$ mm, the alignment error distribution is shown in Fig. 6(b).

3.2.3 Model of alignment error between workpiece and turntable

The alignment error between workpiece and turntable would induce the revolution of the workpiece around the spindle of the turntable. This situation has less impact on the measuring of plane. However, to an aspheric surface, this measurement error must be eliminated. Assuming the

measuring tool and the turntable have been aligned accurately, the influence caused by alignment error between workpiece and turntable would be discussed as follows.

As shown in Fig. 7(a), O is the center of turntable, O_1 is the center of the workpiece, O_2 is the new center of the workpiece after rotating angle θ. The alignment error of the workpiece relative to the turntable is $(\mathrm{d}r,\mathrm{d}\theta)$. The central trace of the workpiece in Fig. 7(a) represents the movement track of the central point of workpiece. When the workpiece center rotated form O_1 to O_2, the measurement error of theoretical measuring point $A(r,\theta)$ can be expressed as

$$\mathrm{d}z_{(\mathrm{d}x,\mathrm{d}y)} = z_A{}' - z_A = \frac{cr'^2}{1+\sqrt{1-(1+k)c^2r'^2}} - \frac{cr^2}{1+\sqrt{1-(1+k)c^2r^2}}, \quad (13)$$

where z_A' is the measured value, z_A is the theoretical value, $\angle O_2OO_1 = \theta$, $\angle O_1OA = \mathrm{d}\theta$, $OO_1 = OO_2 = \mathrm{d}r$, $OA = r$, $O_2A = r' = \sqrt{\mathrm{d}r^2 + r^2 - 2r \times \mathrm{d}r \times \cos(\theta + \mathrm{d}\theta)}$. Equation (13) can be simplified as follows

$$\mathrm{d}z_{(\rho,\theta)} = z_A{}' - z_A = \frac{cr^2 - 2r \times \mathrm{d}r \times \cos(\theta + \mathrm{d}\theta)}{2\sqrt{1-(1+k)c^2r^2}}. \quad (14)$$

Assuming the alignment error $\mathrm{d}r = 1$ mm, $\mathrm{d}\theta = \pi/3$, $r = 20$ mm, the simulation result of the measurement error can be seen in Fig. 7(b). This error distribution is alike with the defocus aberration. It indicates the alignment error between the workpiece and turntable would induce the measurement error distribution which is similar to the defocus aberration.

3.3 Compensation of alignment error

Owing to the measurement error is difficult to be extracted through processing experiment data directly, the alignment error $(\mathrm{d}x,\mathrm{d}y)$ (rectangular coordinates) or $(\mathrm{d}r,\mathrm{d}\theta)$ (polar coordinates) can be separated from the measured data with the help of least square method. Here, the compensation model of alignment error was discussed in the rectangular coordinates. The situation of polar coordinates is similar with the former one.

Take the alignment error model induced by measuring tool and workpiece as an example, the ideal measurement error of point i can be expressed as

$$\mathrm{d}z = \frac{cx_i}{\sqrt{1-(1+k)c^2(x_i^2+y_i^2)}}\mathrm{d}x + \frac{cy_i}{\sqrt{1-(1+k)c^2(x_i^2+y_i^2)}}\mathrm{d}y. \quad (15)$$

Assigning: $S = \mathrm{d}x$, $T = \mathrm{d}y$, and

$$\begin{cases} s_i = \dfrac{cx_i}{\sqrt{1-(1+k)c^2(x_i^2+y_i^2)}}, \\ t_i = \dfrac{cy_i}{\sqrt{1-(1+k)c^2(x_i^2+y_i^2)}}. \end{cases} \quad (16)$$

Then, Eq. (15) would be rewritten as

$$\mathrm{d}z = s_iS + t_iT. \quad (17)$$

Define $W(S,T)$ as Eq. (18), where $\mathrm{d}z'$ denotes the actual measurement error.

$$W(S,T) = \sum_{i=1}^{n}[\mathrm{d}z' - \mathrm{d}z]^2 = \sum_{i=1}^{n}[\mathrm{d}z' - (s_iS + t_iT)]^2. \quad (18)$$

Based on the least square method, Eq. (18) should

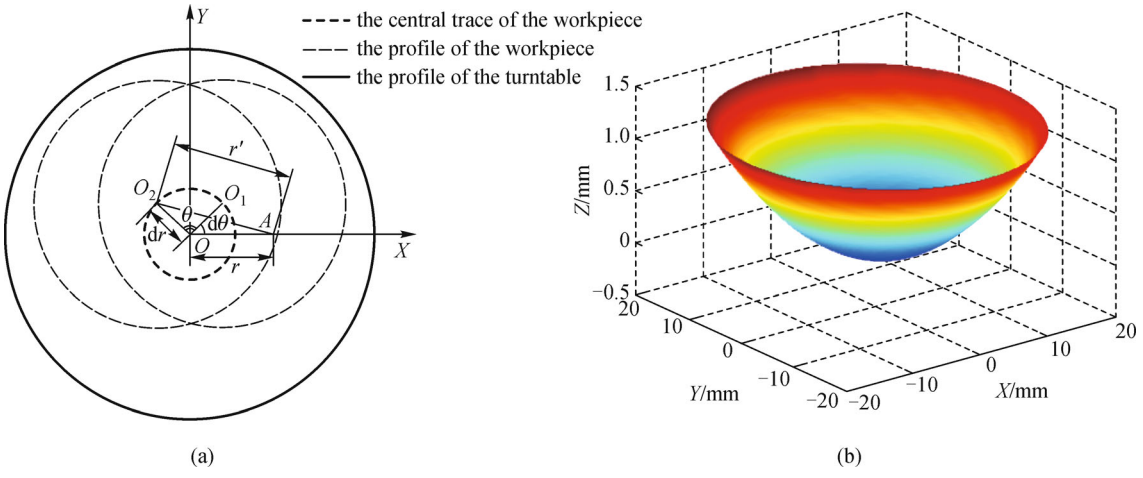

Fig. 7 Model of alignment error between workpiece and turntable. (a) Geometrical relationship among alignment errors; (b) 3D distribution of alignment error

satisfy Eq. (19), which is simplified as Eq. (20). Solve it with numerical computation method, S and T can be obtained, then we can get dz and the final surface form.

$$\frac{\partial W}{\partial S} = \frac{\partial W}{\partial T} = 0, \tag{19}$$

$$\begin{vmatrix} \sum s_i^2 & \sum s_i t_i \\ \sum t_i s_i & \sum t_i^2 \end{vmatrix} \begin{vmatrix} S \\ T \end{vmatrix} = \begin{vmatrix} \sum \mathrm{d}z' s_i \\ \sum \mathrm{d}z' t_i \end{vmatrix}. \tag{20}$$

4 Experiment of surface measurement

4.1 Measuring force test

The digital length gauge MT60 has three kinds of measuring force to be selected, includes 1.00 N, 1.25 N, 1.75 N. Large measuring force would induce the deformation of the measuring tool and the workpiece. On the contrary, the measuring tool cannot contact with the workpiece adequately due to the existence of the mote.

To study the influence of the measuring force, five groups of experiments have been conducted under the same condition. The measuring tool adopts half-retraction mode, so that the experimental time can be reduced. The experimental results are shown in Fig. 8. It can be seen that, the absolute value of the output value is proportional to the measuring force. Therefore, the measuring force should be kept invariable during the measurement in order to eliminate its effect.

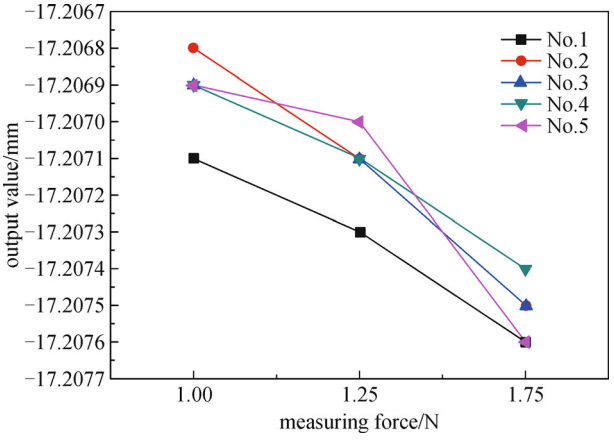

Fig. 8 Influence of e measuring force on output value

4.2 Stability test

To verify the stability of PMI700, two sets of experiments have been conducted to measure a transversal on a convex and a plane mirror, respectively. The sagittal height of the convex mirror is 6.85 mm, and the length of the measured line is 100 mm. 100 points have been measured with an interval of 1 mm. The experimental result is shown in Fig. 9(a). Another measuring object is a plane mirror with the sagittal height of 0.073 mm, which was measured 120 times along a transversal of 120 mm in length. The measuring result can be seen in Fig. 10(a). Each experiment has repeated five times.

The differences between each group shown in Figs. 9(b) and 10(b) are calculated by the rear four groups subtracting from the first group. It can be found each set has a similar variation tendency, and the peak to valley (PV) of each set are 2 and 1 μm, respectively, the standard deviation is within 0.5 μm. The PV and standard deviation of each group are listed in Tables 2 and 3, respectively.

The experimental results indicated the well stability of PMI700. In addition, the deviation between each group is caused by the variation of the environment, such as the temperature. Here, the influence of the temperature would be discussed in the next section.

4.3 Temperature test

Silica glass was selected due to its insensitive to the temperature. On account of the resolution of the thermometer, the measuring datum corresponding to one temperature is averaged by five values. The relationship between measuring value and temperature was obtained in Fig. 11. It can be seen that the standard deviation of temperature variation is 0.647 μm, PV is 1.9 μm, and the rate of temperature change is 2.8 μm/°C. Thus, the variation of the temperature has a significant influence on the measuring result. The temperature should be controlled during the measurement, especially for the K9 glass which is sensitive to the temperature. To reduce the influence of the temperature, the measurement should be conducted in a homothermal environment, and the preheating of PMI700 is also necessary.

4.4 Surface topography measurement by PMI700

Through the discussion of the influence factors, several kinds of optical elements were measured by PMI700 after compensating the influence of tool radius error, alignment error and temperature. The measuring results were compared with the data measured by interferometer.

Figure 12 shows the surface topography of a plane mirror with diameter of 96 mm. For the plane mirror, the raw data (Fig. 12(a)) only include tilt error that have no need to eliminate any other errors. After removing the tilt error, the measurement data of PMI700 (Fig. 12(b)) is, PV = 4.423λ, RMS = 0.944λ. The result of Zygo interferometer (Fig. 12(c)) is, PV = 4.593λ, RMS = 0.774λ. The direct subtraction of these two results is shown in Fig. 12(d), which indicates PV is 0.60037λ, RMS is 0.9412λ. It can be

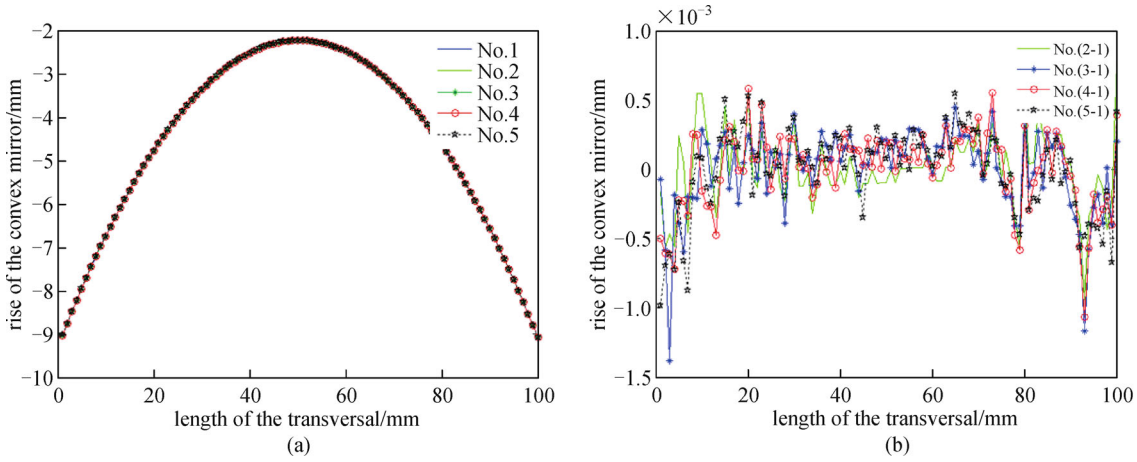

Fig. 9 Measuring result of a transversal on convex mirror. (a) Measuring data; (b) differences between repeated measuring data

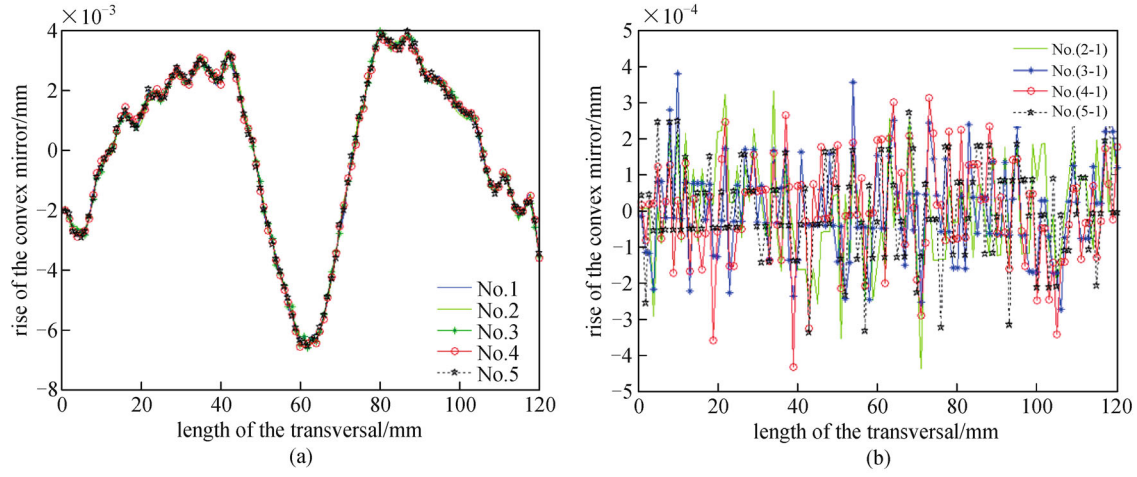

Fig. 10 Measuring result of a transversal on plane mirror. (a) Measuring data; (b) differences between repeated measuring data

Table 2 PV and standard deviation of convex mirror

	No. (2-1)	No. (3-1)	No. (4-1)	No. (5-1)
standard deviation/μm	0.26582	0.30130	0.28665	0.31796
PV/μm	1.7	1.9	1.6	1.5

Table 3 PV and standard deviation of plane mirror.

	No. (2-1)	No. (3-1)	No. (4-1)	No. (5-1)
standard deviation/μm	0.14286	0.13586	0.14459	0.13637
PV/μm	0.77	0.65	0.75	0.63

seen, the measurement accuracy of PMI700 can satisfy the demand in the condition of the accuracy limitation of the measuring head (±0.5 μm).

Figure 13 is the measuring result of a hyperboloidal mirror with conic constant $k = -1.77$, vertex curvature radius $R = 330$ mm. In Fig. 13(a), the data after removing tilt error have been provided. It can be seen the error shape is caused by the alignment error of workpiece and

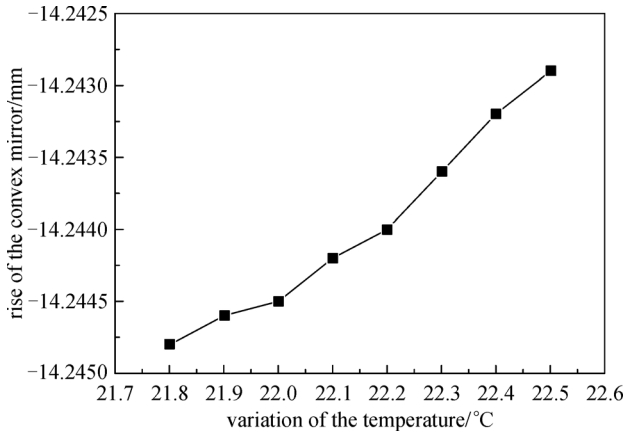

Fig. 11 Influence of temperature on measuring value of PMI700

turntable, as well as the alignment error of measuring tool and turntable. Based on the alignment error model in Section 3.3, the final result after eliminating all alignment errors is shown in Fig. 13(b), which indicates PV is 2.22684λ, RMS is 0.30334λ. The result of sub-aperture stitching (Fig. 13(c)) is, PV = 1.79λ, RMS = 0.23λ. The direct subtraction of these two results (Fig. 13(d)) is, PV = 0.85766λ, RMS = 0.098008λ, which indicates the data obtained by PMI700 is basically identical with the result of interferometer.

5 Conclusions

In this paper, the profile measurement of aspherics by a three-dimensional profile measurement system (PMI700) was studied in detail. The measurement error induced by radius of measuring tool, alignment error and the temperature variation were analyzed respectively. One quantitative method was presented for the compensation of the measuring tool radius. Through geometry analysis, the models of measurement error induced by alignment error were constructed, and the error distribution can be visually observed by simulation. In addition, an alignment error compensation model was presented on the basis of the least square method to reduce the measurement error. Plane mirror and non-uniform hyperboloidal mirror were measured by PMI700. The results compared with the data measured by interferometer shown, the measurement accuracy of PMI700 can satisfy the requirements.

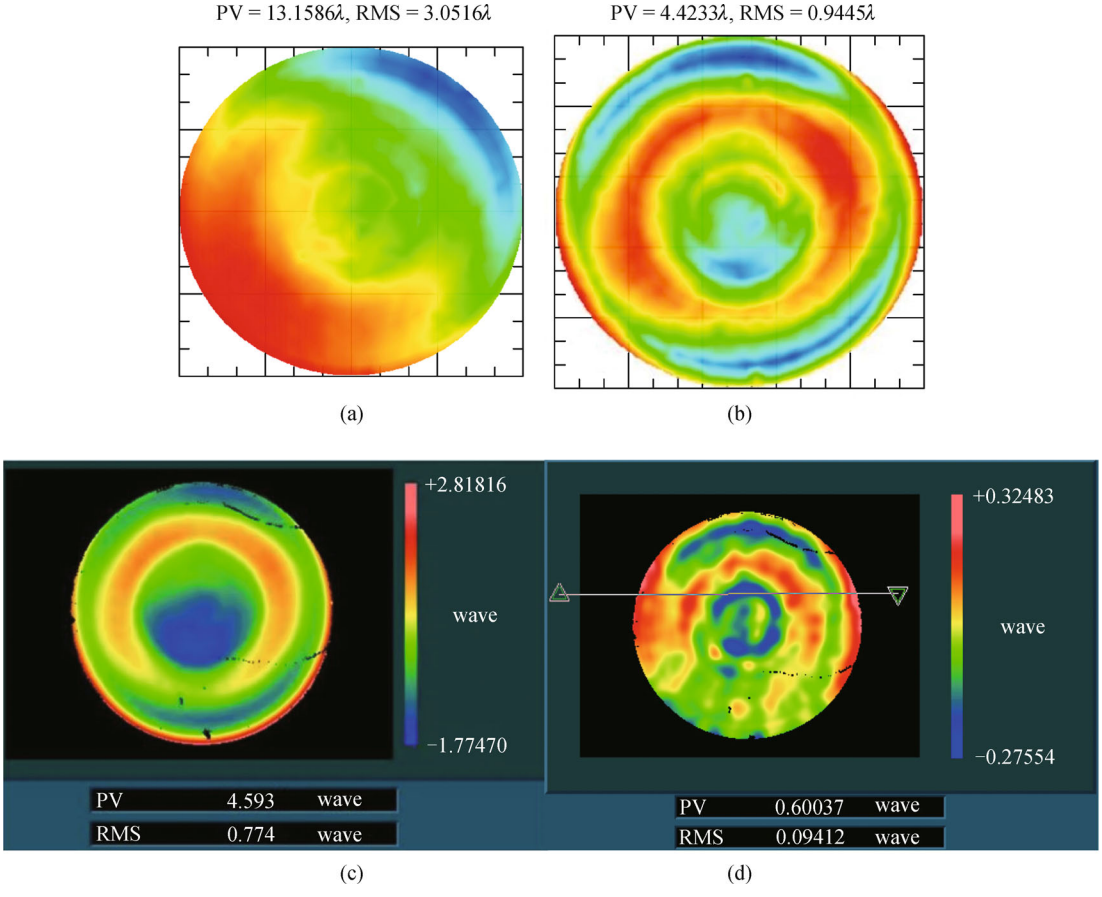

Fig. 12 Plane mirror measurement. (a) Raw data; (b) measuring result obtained by PMI700; (c) measuring result obtained by Zygo; (d) direct subtraction of measurement results of PMI700 and Zygo

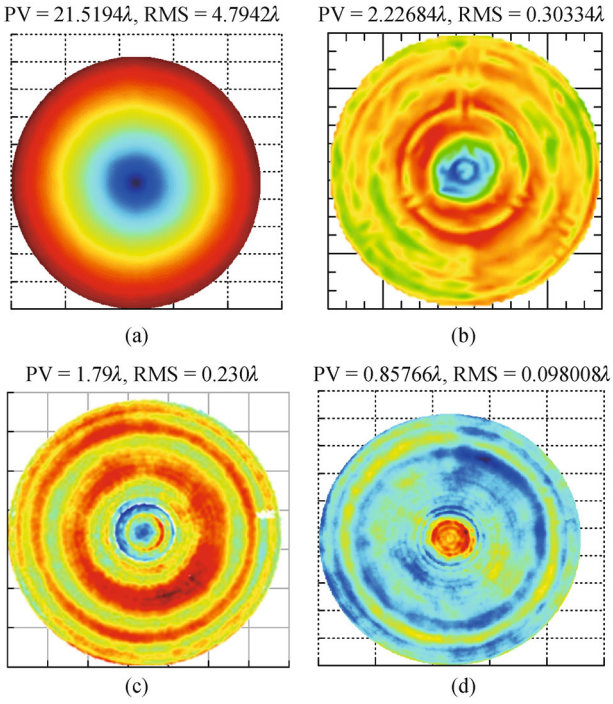

Fig. 13 Hyperboloidal mirror measurement. (a) Raw data after removing tilt error; (b) measuring result obtained by PMI700; (c) measuring result obtained by sub-aperture stitching; (d) direct subtraction of measurement results of PMI700 and sub-aperture stitching interferometer

Acknowledgements This work was supported by the National Natural Science Foundation of China (Grant Nos. 61128012, 61061160503 and 61222506), the Key Laboratory of Photoelectronic Imaging Technology and System, BIT, Ministry of Education of China (No. 2013OEIOF06).

References

1. Zamkotsian F, Dohlen K, Lanzoni P, Mazzanti S P, Michel M L, Buat V, Burgarella D. Knife-edge test for characterization of sub-nanometer deformations in micro-optical surface. Proceedings of SPIE, Optical Manufacturing and Testing III, 1999, 3782: 328–336
2. Hernández-Gómez G, Malacara-Hernández Z, Malacara-Hernández D. Hartmann tests to measure the spherical and cylindrical curvatures and the axis orientation of astigmatic lenses or optical surfaces. Applied Optics, 2014, 53(6): 1191–1199
3. Dickson L D. Ronchi ruling method for measuring Gaussian beam diameter. Optical Engineering (Redondo Beach, Calif.), 1979, 18 (1): 180170
4. Zhou P, Burge J H. Optimal design of computer-generated holograms to minimize sensitivity to fabrication errors. Optics Express, 2007, 15(23): 15410–15417
5. Takasaki H. Moiré topography. Applied Optics, 1970, 9(6): 1467–1472
6. Chen S, Li S, Dai Y, Zheng Z. Testing of large optical surfaces with subaperture stitching. Applied Optics, 2007, 46(17): 3504–3509
7. Kühn J, Colomb T, Montfort F, Charrière F, Emery Y, Cuche E, Marquet P, Depeursinge C. Real-time dual-wavelength digital holographic microscopy with a single hologram acquisition. Optics Express, 2007, 15(12): 7231–7242
8. Barrientos B, Martínez-CelorioR A, López L M, Dirckx J J J, Cywiak M. Measurement of out-of-plane deformation by combination of speckle shearing interferometry. Optik (Stuttgart), 2004, 115 (6): 248–252
9. Goodwin E P, Wyant J C. Field Guide to Interferometric Optical Testing. Bellingham, WA: SPIE Press, 2006
10. Breidenthal R S. Measurement of large optical surfaces for fabrication using a non-optical technique. Proceedings of SPIE, Large Optics II, 1992, 1618: 97–103
11. Comley P, Morantz P, Shore P, Tonnellier X. Grinding metre scale mirror segments for the E-ELT ground based telescope. CIRP Annals-Manufacturing Technology, 2011, 60(1): 379–382
12. Gray C, Baker I, Davies G. Fast manufacturing of E-ELT mirror segments using CNC polishing. Proceedings of SPIE, Optical Manufacturing and Testing X, 2013, 8838: 88380K
13. Su P, Oh C J, Parks R E, Burge J H. Swing arm optical CMM for aspherics. Proceedings of SPIE, Optical Manufacturing and Testing VIII, 2009, 7426: 74260J
14. Su P, Wang Y H, Oh C J, Parks R E, Burge J H. Swing arm optical CMM: self-calibration with dual probe shear test. Proceedings of SPIE, Optical Manufacturing and Testing IX, 2011, 8126: 81260W
15. Jing H, King C, Walker D. Simulation and validation of a prototype swing arm profilometer for measuring extremely large telescope mirror-segments. Optics Express, 2010, 18(3): 2036–2048
16. Jing H, King C, Walker D. Measurement of influence function using swing arm profilometer and laser tracker. Optics Express, 2010, 18

(5): 5271–5281

17. Chen F J, Yin S H, Huang H, Ohmori H, Wang Y, Fan Y F, Zhu Y J. Profile error compensation in ultra-precision grinding of aspheric surfaces with on-machine measurement. International Journal of Machine Tools & Manufacture, 2010, 50(5): 480–486

Xu Ye is a master at Beijing Institute of Technology and she received her bachelor degree at Xi'an Technological University in 2012. Her current research is in the area of optical processing and testing.

Haobo Cheng is a current Professor Doctoral supervisor in Beijing Institute of Technology. He received his Ph.D. degree in Changchun Institute of Optics, Fine Mechanics and Physics, Chinese Academy of Sciences. He is also the dean of research institute in Zhuhai and director at the joint research center for opto-mechatronics engineering. The present research work is precision ultra-precision manufacturing and testing.

Zhichao Dong is a doctor at Beijing Institute of Technology, where he also got his master degree. And he received his bachelor degree at Qingdao University. He engaged in the fabrication of an off-axis aspherical mirror with a lager-aperture.

Hon-Yuen TAM obtained his B.Sc. degree from Georgia Institute of Technology, M.Sc. and Ph.D. degrees from Stanford University, all in mechanical engineering. He is a Chartered Engineer and a fellow of the Institution of Measurement and Control, UK. He is a University Lecturer in City University of Hong Kong and his research interest is surface finishing automation and numerical control.